

ARTICLE OPEN



A paper-based self-inductive folding displacement sensor for human respiration and motion signals measurement

Junwen Zhu¹, Yanshen Jia¹, Mengmeng Li¹, Zhanxuan Zhou², Yinghao Chen³, Qiang Liu^{1,4} and Xing Yang^{1,4}✉

Flexible sensors have recently attracted much attention for potential applications in motion measurement and wearable health monitoring. In this paper, an environment-friendly, economic, and high-performance paper-based self-inductive folding displacement sensor (PSIFS) was proposed, with displacement resolution of 20 μm and wide measurement range of 43.2 mm. The sensor sensitivity could reach 4.44% mm^{-1} with the maximum deviation of 0.00904 in experiments. The sensing mechanism based on inductance variation due to three-dimensional deformation of planar inductor coil and structural design principle under two dimensions of sensitivity and size were proposed and studied. The folding method to enhance sensitivity was proposed and 3 times sensitivity enhancement could be achieved by once folding. Multiple breathing states and motion states of the human joints could be recognized. The proposed simple paper-based sensor, folding method to increase sensitivity, and structural design model may provide a way for the research of flexible sensors.

npj Flexible Electronics (2022)6:67; <https://doi.org/10.1038/s41528-022-00198-0>

INTRODUCTION

Flexible sensing technology has shown a great application potential in human physiological signal measurement^{1–3}, flexible robots^{4–6}, and wearable electronic devices^{7–9}, and been widely studied by researchers. Flexible sensors with resistive^{10–12}, capacitive^{13–16}, inductive^{17–20}, triboelectric²¹ and other sensing principles have been used to measure the signals of mechanical quantity. Among the sensors with different principles, the requirement of inductive sensors for substrate and coil materials are relatively low, and inductive sensors could also easily meet the requirements of wireless measurement and signal transmission. According to the principle of electromagnetic induction and mutual inductance, the inductive sensors could be used to measure displacement, pressure and other physical quantities with high sensitivity. These advantages make the inductive sensors have great potential in flexible sensing of mechanical quantity.

At present, three main types of flexible inductive sensors are used widely as eddy current, mutual-inductive and self-inductive sensors, respectively. Among them, the eddy-current flexible sensors have been researched the most. For example, tactile sensor composed of iron film and planar coil antenna at the bottom was fabricated on the basis of human hairy microstructure, which could characterize the pressure on the sensor by the changes in the resonant frequency of the induced coil¹⁸. Liquid metal encapsulated in silica gel was made as the sensing element and four induced coils as the sensor array to achieve deformation monitoring in three-dimensional (3D) directions²². Besides, mutual-inductive sensors are used to change mutual-induced electromotive force through mutual position change between two electrified coils to realize the change in inductance value. For example, a kind of coaxial inductor structure with inner and outer cylindrical shapes was designed. The rotation angle can be monitored using the mutual inductance between the inductors²³. In principle, at least two parts separated from each other are required

in eddy current sensors and mutual-inductive sensors. The high structural complexity is not convenient for wearable application.

By comparison, self-inductive sensors achieve the sensing of mechanical quantity based on the structure change. The sensing function could be realized by only one coil, which shows the better structural stability compared to the other two kinds of inductive sensors. Therefore, it is more suitable for human physiological signal monitoring and other application scenarios. For example, sandwich structure of flexible polyester film-coil-Metglas magnetostrictive ribbon was fabricated to realize angle monitoring and was able to monitor many different joints motion²⁴. A kind of solenoid type of inductive sensor was fabricated in the previous report²⁵. When the coil is bent, the inductance value changes due to the change of the angle between coils, and this sensor could be used to detect finger bending.

However, most flexible sensors at present require nanomaterials and complex fabrication processes, which greatly limit the application of flexible sensors. Finding the balance between the performance and cost of flexible sensors will be one of the possible trends in future flexible electronics research. In addition, although self-inductive sensors have many advantages, there is not much research available. The sensing model and structural design principle need to be further researched. The performance of sensors should also be further enhanced to meet more applications. Therefore, we hope to design a self-inductive sensor with high performance, low cost and suitable for a variety of applications.

In terms of substrate material, PDMS^{26–28}, PI^{29,30} and other polymer material are often used in flexible electronics. However, the high cost and complex processing process cannot meet the requirement of low-cost sensors. As a kind of polymer material with fiber structure, paper is characterized by low price and environmental friendliness, and there are lots of research about sensors based on flexible paper substrate^{31–34} recently. Therefore, the paper-based displacement sensor based on self-inductive

¹The State Key Laboratory of Precision Measurement Technology and Instruments, Department of Precision Instrument, Tsinghua University, Beijing 100084, China. ²School of Materials Science and Engineering, University of Science and Technology Beijing, Beijing 100083, China. ³School of Electromechanical and Automobile Engineering, Yantai University, Yan Tai 264005, China. ⁴Key Laboratory of Photonic Control Technology, Ministry of Education, Tsinghua University, Beijing 100083, China.

✉email: yangxing@tsinghua.edu.cn

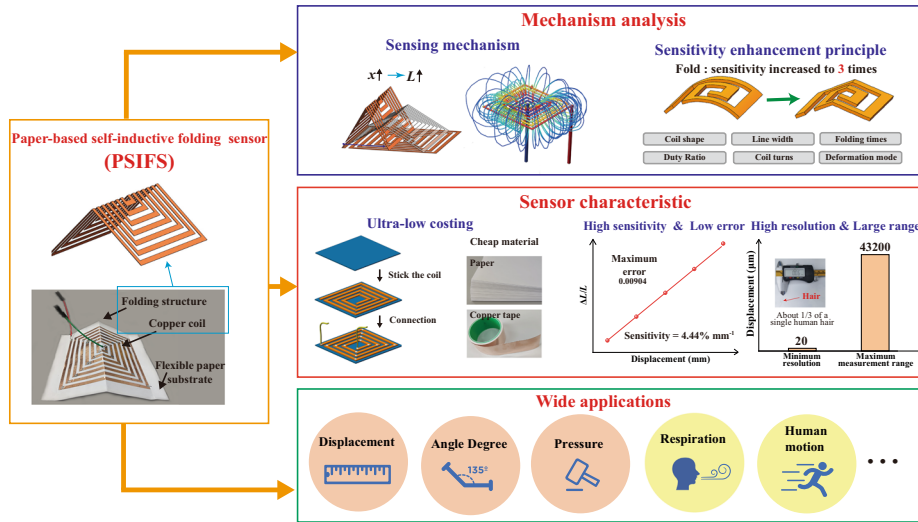


Fig. 1 Schematic of PSIFS. The structure, mechanism, characteristics and applications of PSIFS.

principle was researched in this paper. In terms of applications, such as pressure, angle degree variation and some other physical quantities can be converted into displacement for measurement^{35,36}. Therefore, displacement sensors can achieve the measurement of multiple physical quantities and suitable for multiple human respiration modes and motion signals monitoring. In terms of increasing sensitivity of flexible displacement sensors, adding additional materials^{37–39} and fabricating complex structure^{40–42} are the most commonly used methods. Although the sensitivity enhancement can be achieved by several times, the cost and manufacturing difficulty of the sensor need to be further increased. We hope to utilize the advantages of easy to be folded in paper materials, and use the simple folding operation to achieve sensitivity enhancement.

In this paper, PSIFS with characteristics of simple manufacturing process and low cost is designed for displacement measurement. It could also be used for detecting angle degree, pressure, respiration signal, and human motion signals. The schematic in this article is shown in Fig. 1. PSIFS can be fabricated by the common paper material and copper tape, without complex and expensive fabrication process. Therefore, the cost of sensors is extremely low and thousands of sensors could be fabricated within 1 dollar. Although the sensor cost is low, high sensitivity, wide measurement range and other good performance could be achieved. The working principle of PSIFS is analyzed theoretically and verified by finite element simulation and experiments. The method of introducing folding structure is proposed to improve self-inductive sensor sensitivity. The influences of several other structural parameters of coils, including coil shape, line wide, folding times, duty ratio and number of turns on the sensitivity of the sensors, are analyzed to determine the optimal structure. The design principle of structural parameters under sensitivity-size two dimensions is also proposed. Sensitivity, minimum resolution, response time, robustness and other parameters of PSIFS are tested to verify its sensing capability. PSIFS has the properties of high sensitivity, low error, high resolution and large measurement range. In addition, PSIFS could convert other physical quantities into the displacement change to achieve measurement, which make PSIFS could be used to monitor finger expansion and joint rotation at different motion speeds, as well as to distinguish different breathing modes.

RESULTS

Analysis of sensor sensing mechanism

In this work, the displacement measurement of PSIFS can be attempted to be realized by deformation in three-dimensional of planar spiral coil. The basic structure of the planar coil is shown in Fig. 2a. Through angle-side division, the inductance coil could be subdivided into the comprehensive performance of self-inductance and mutual inductance of each rectilinear wire^{43,44}. The Eqs. 1 to 5 are obtained from references^{43,44}. The overall inductance of the coil, L_s , can be expressed by Eq. 1.

$$L_s = \sum_{i=1}^{4N} L_i + \sum_{i=1}^4 \sum_{j=1-i}^N M_{2i-1, 2i+2j-1} + \sum_{i=1}^4 \sum_{j=\frac{3}{2}-i}^N M_{2i-1, 2i+2j-1} \quad (1)$$

L_i refers to the inductance value of the rectilinear wire numbered as i , and M_{ij} refers to the mutual inductance between two parallel wires numbered as i and j . Each of them can be expressed using Eqs. 2 and 3.

$$L_i = 0.002l_i \{ \ln[2l_i / (w + t)] + 0.50049 + [(w + t) / 3l_i] \} \quad (2)$$

$$M_{ij} = \frac{M_{j+a} - M_a}{2} + \frac{M_{j+b} - M_b}{2} \quad (3)$$

M_i is an operator in the intermediate process and can be expressed as Eq. 4, and GMD is a parameter related to geometric mean distance and can be expressed as Eq. 5.

$$M_i = 2l_i \cdot \left\{ \ln \left[\frac{l_i}{\text{GMD}} + \sqrt{1 + \left(\frac{l_i}{\text{GMD}} \right)^2} \right] - \sqrt{1 + \left(\frac{\text{GMD}}{l_i} \right)^2} + \frac{\text{GMD}}{l_i} \right\} \quad (4)$$

$$\ln \text{GMD} = \ln s - \sum_{n=1}^{\infty} \left[\frac{\left(\frac{s}{w} \right)^{-2n}}{12 \cdot \sum_{i=1}^n i^2} \right] \quad (5)$$

w and t refer to the width and thickness of the rectilinear wire, respectively. l_i refers to the length of the wire numbered i . s refers to the space position distance between wires. a and b refer to the differences in the length between two parallel wires on each side. The relationship among different parameters is shown in Supplementary Fig. 1.

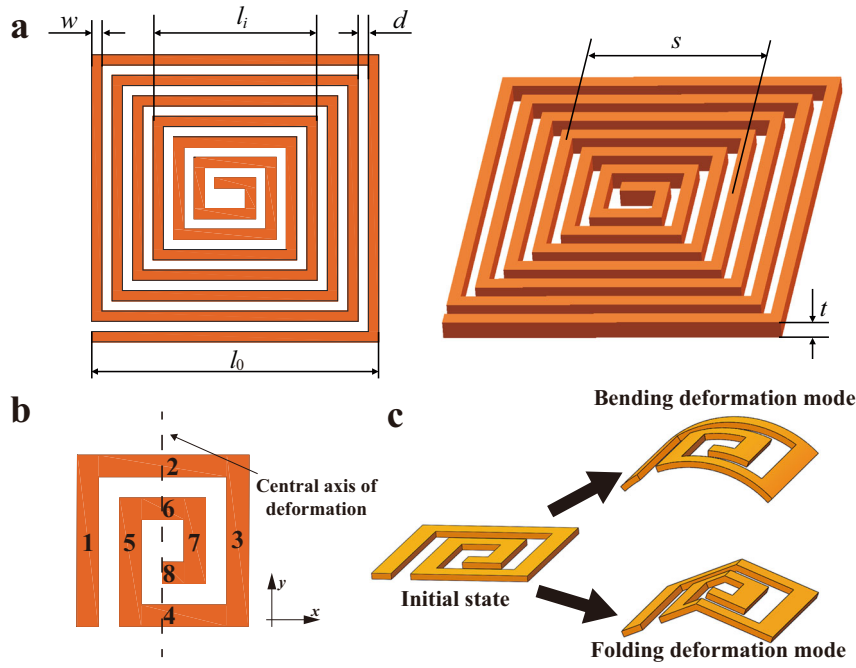


Fig. 2 Mechanical model of PSIFS. a Schematic of the basic structure parameters of coils in PSIFS. **b** Schematic of simplified less-turn model. **c** Schematic of bending and folding deformation modes.

In accordance with Eq. 5, the relationship between GMD and s could be obtained.

$$GMD' = GMD \cdot \left(\frac{1}{s} + \sum_{n=1}^{\infty} \frac{w^{2n}}{12 \cdot \sum_{i=1}^n i^2 \cdot s^{2n+1}} \right) \quad (6)$$

In accordance with Eq. 6, the derivative of GMD to s is constantly positive. Therefore, a positive correlation exists between GMD and s , so the analysis of the variation relationship between L_s and s is similar to that in the analysis between L_s and GMD. λ is defined as $\lambda = \frac{l}{GMD}$ in the calculation. Because of that the wire length l remains nearly unchanged in the bending and folding processes, λ has a unique and definite correspondence to GMD. The mutual inductance could be rewritten as follows:

$$M_l = 2l \cdot \ln \left[\lambda + \sqrt{1 + \lambda^2} \right] - \sqrt{1 + \frac{1}{\lambda^2}} + \frac{1}{\lambda} \quad (7)$$

The coil model with less turns is adopted to simplify the analysis process in this paper. For the coil with more turns, only the increase in the amount of calculation occurs, while the basic principle and calculation process are consistent with analysis process of less turns. The simplified less-turn model is shown in Fig. 2b. The self-inductive sensor proposed in this paper could realize bending and folding two deformation modes, as shown in Fig. 2c. According to Eq. 1, the total inductance L_s is associated with the self-inductance of all wires and mutual inductance between wires. l_i , w , and t do not change with the deformation in the process of displacement change. According to Eq. 2, the self-inductance of all wires does not change. Therefore, the factor affecting the inductance of the coil is the mutual inductance between the wires in the coil due to the change of s .

In the process of displacement changing, the relative position distance of the sensor in the y direction does not change, which has no effect on the inductance of the sensor. Therefore, only the change in the relative position in the x direction should be discussed. For the basic model shown in Fig. 2b, wires numbered as 2, 4, 6, and 8 are at the y direction so out of the consideration.

Wires numbered as 1 and 5, 3 and 7 have a consistent current direction. Both in folding and bending deformation, their position distance does not change so the mutual inductance does not change as well. However, the current direction in the combinations of wires numbered as 1 and 3, 1 and 7, 5 and 3, and 5 and 7 is the opposite, so the mutual inductance is negative.

Equation 3 shows that the change in the mutual inductance between two wires is associated with mutual inductance difference $M_{m+p} - M_p$, namely ΔM . Therefore, the relationship between λ and ΔM is analyzed to obtain the sensor inductance variation in the deformation process. Through two derivations of λ , the following equation could be obtained:

$$M'' = - \frac{(\sqrt{1 + \lambda^2} - 1)^2}{\lambda^3 \cdot \sqrt{1 + \lambda^2}} \quad (8)$$

The first-order derivative of the formula is a constantly positive value, and the second-order derivative is a negative value, indicating a negative correlation between ΔM and λ . In addition, due to the inversely proportional relationship between λ and GMD, when GMD decreases, ΔM also decreases. In accordance with Eq. 3, the mutual inductance decreases. Given the positive correlation between GMD and s , the sensor inductance value gradually decreases with the distance between both ends of the coil decreases according to Eq. 1.

To further verify the above relationship, the finite element analysis was used to simulate the electromagnetics of the fabricated inductance coil and calculate the inductance values when the inductance coil deformed. In the simulation process, the folding deformation mode was taken as an example. The model structure is shown in Fig. 3a. A planar rectangular coil model was constructed and two cuboids with high depth-to-width ratio was set to simulate the connection of the leading wires. An AC voltage with amplitude of 1 V and frequency of 1 MHz was applied on both ends of the coil. The voltage distribution in the inductance coil and the distribution of magnetic induction line in the surrounding space are shown in Fig. 3a. The measurement results

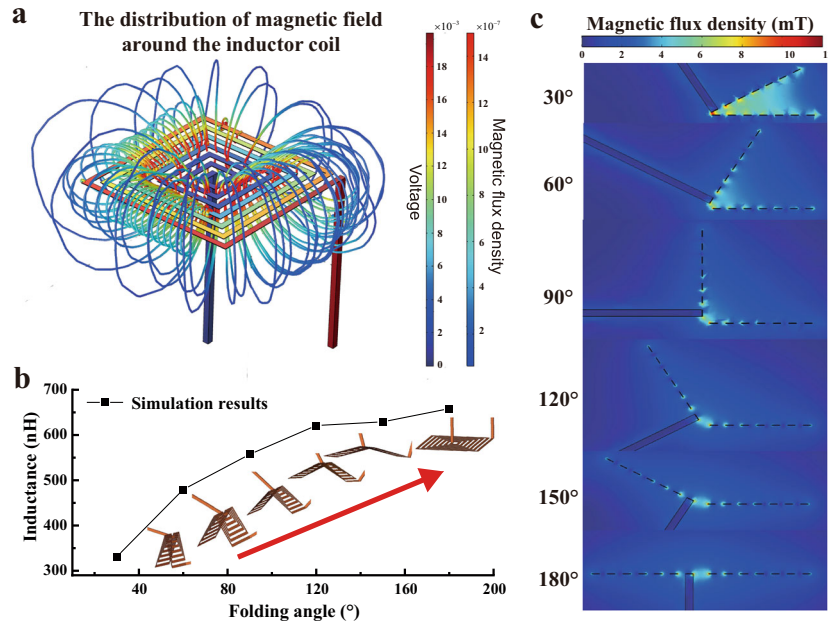


Fig. 3 The sensing simulation of PSIFS. **a** Simulation results of the voltage and magnetic line distribution. **b** Variation curve of inductance values in different states. **c** Magnetic flux density distribution in different states.

at different bending angle of the sensor, which means different displacement, are shown in Fig. 3b. With the gradual unfolding of the sensor, the displacement increases gradually. The sensor inductance value shows a gradually increasing trend with displacement change, which is consistent with the changing trend derived from the numerical analysis. It verifies that the correctness of the relational model deduced previously and proposed self-inductive sensor could be used for displacement or angle measurement. Figure 3c shows the finite element simulation result of magnetic flux density distribution in the surrounding air domain when sensor in different displacement positions.

According to above analysis results, a simple fabrication process is designed. The inductance of sensor changes with the distance of space position distance s , while substrate material and coil material nearly do not affect the performance. Therefore, the common paper in life was used as the flexible substrate, and the copper foil tape was used as the conductive layer to fabricate coil. The fabrication process and physical picture of each stage in the process are shown in Supplementary Fig. 2.

The paper material is interwoven by fibers, so it is easier to produce crease to form folding structure than other flexible materials. Through the introduction of folding structure, the space position distance s between the straight wires could change under the same displacement variation of the sensor, which means the sensor sensitivity could be further improved. The sensor sensitivity in bending and folding deformation modes was analyzed and contrasted. Equations 1 and 8 show a positive correlation between the inductance value and s . Therefore, the sensitivity could be determined by analyzing the change in the variation of s caused by folding or bending deformation mode. The sectional drawings and the parameter definitions in the two modes are shown in Fig. 4a. The deformation of inductance coil in bending and folding modes was calculated in detail in the Supplementary Note 1. The s_{bend} and s_{fold} between two parallel rectilinear wires are as follows:

$$s_{\text{bend}} = \frac{l_0}{a} \cdot \sin\left(\frac{a+b}{l_0} \cdot a\right), \quad \text{where } \frac{\sin a}{a} = \frac{l_0 - \Delta x}{l_0} \quad (9)$$

$$s_{\text{fold}} = \sqrt{(a-b)^2 + 4ab \cdot \left(\frac{l_0 - \Delta x}{l_0}\right)^2} \quad (10)$$

The total length of the sensor is set to 100 mm and five groups of different a and b are selected to represent the position relationship between groups of straight wires with different deformation. These parameter settings could cover most of the wire combinations comprehensively. The calculation was carried out in accordance with Eqs. 9 and 10, and the results are shown in Fig. 4b. The wires separation distance in the folding deformation mode was smaller than that in the bending mode. That is, the s changes more considerably in the folding deformation mode, with larger inductance variation in the same displacement variation. This indicates that the sensor could have higher sensitivity in the folding deformation mode than the bending deformation mode.

The physical pictures of the sensor in the initial state and under two deformation modes are shown in Fig. 4c. Two groups of sensors with the same size were fabricated, three for each group, to test the sensitivity in two deformation modes. The sensitivity in the folding deformation mode is approximately 3 times of that in the bending deformation mode, as shown in Fig. 4d. Only by once folding, the sensitivity can be increased to 3 times. Compared with other performance improvement methods of displacement sensor in the previous references^{37–42}, our method can achieve similar enhancement result, but is a very simple one without adding additional materials or fabricating complex structure.

Effect of the multiple structure parameters of planar inductor coil on the sensitivity

According to the above analysis, the sensitivity of PSIFS is positively correlated with the change of s . Due to that different sensor structure parameters will affect the value variation of s , the effect of various structural parameters on sensor sensitivity are analyzed and verified by experiments. For the planar induction coil, the following structural parameters determine the coil configuration: coil shape, duty ratio (DR), coil turns (n), line width (w). DR is defined as the ratio of the line width of the inductor to the air gap, which means w/d .

To further distinguish the sensitivity of PSIFS with different sizes in the displacement measurement, the sensitivity of the relative displacement change (the ratio of the displacement to be measured in the initial length of the sensor, $\frac{\Delta L/L_0}{\Delta x/l_0}$) is used in

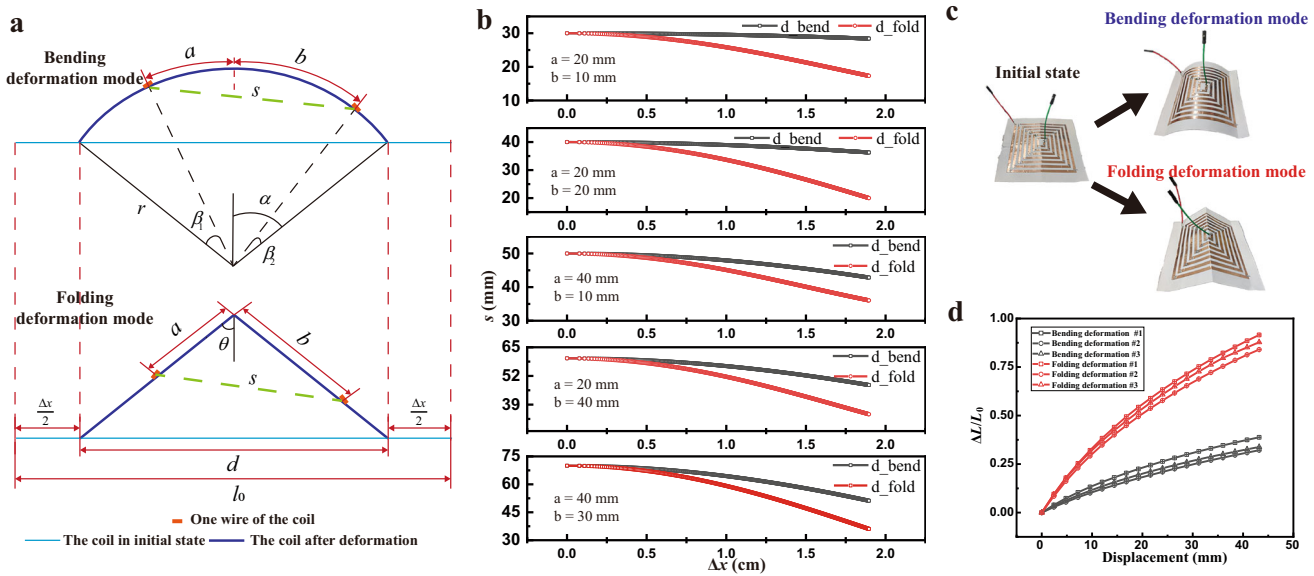


Fig. 4 Comparison of folding and bending deformation modes. **a** Section diagram and parameter meanings of bending and folding deformation modes. **b** Simulation results of position relationship under different wire spacing deformations. **c** PSIFS in bending and folding deformation modes. **d** Measurement results of the sensitivity in bending and folding modes.

comparing sensors with different parameters. ΔL refers to the variation of relative inductance. Δx refers to the displacement to be measured. L_0 and l_0 refer to the initial inductance value of the sensor and initial sensor length, respectively. For different structural parameters, three sensors were fabricated respectively to get the relation between the structural parameter and sensitivity.

First, the relationship between the shape of inductance coil and the sensitivity of the sensor is analyzed. The commonly used polygon coil shapes in PCB, integrated circuit, and other fields at present include regular quadrilateral, regular hexagon, and regular octagon^{45,46}. In this paper, the inductance coils in the shapes of these three were fabricated. Schematics of the sensors in three shapes are shown in Fig. 5a. All parameters except for coil shape, were fixed to $n = 6.5$, $w = 1$ mm, and $DR = 1$ to ensure variable isolation. The sensitivity of regular quadrilateral sensors is the highest with approximately 1.51 times of regular octagonal sensors and 2.37 times of regular hexagonal sensors. Therefore, the coil in regular quadrilateral shape is used in analyzing the effect of other parameters on sensitivity. In the process of sensor deformation, the main mutual inductance change is the directly parallel straight wires, and the mutual inductance of wires with other relative position relationship unchanged or changed barely. From the perspective of simplified model, the larger length of opposite parallel straight wires could increase the sensor sensitivity. Therefore, compared with coils of other shapes, regular square coil has higher sensitivity.

Second, the effect of DR on the sensitivity is analyzed. The following conditions were set: $n = 6.5$, $w = 1$ mm, and $DR = 2, 1$, and 0.5 . Schematics of the sensors under different parameter settings are shown in Fig. 5b. Meanwhile, three sensors were fabricated under each group of parameter settings to measure the sensitivity in the lifting and returning. The results reveal that with the decreasing of DR, the sensitivity of the sensor presented a rising trend. The reason is that when reducing DR, the distance between the parallel straight wires of the coil is increased, which means the length of the straight wire will also get longer. Therefore, the sensitivity enhancement can be achieved by reducing DR, while the size of sensor will also increase in this case.

Third, the effect of the number of turns on sensitivity was analyzed. All parameters, except for the number of turns n , were fixed to $w = 1$ mm and $DR = 1$. A schematic of the different turns of coils is shown in Fig. 5c. With the increase in turns, more straight wire pairs producing the mutual inductance effects are introduced. Therefore, the mutual inductance of each part of the sensor changes considerably in the same displacement change, and the sensitivity increases. The sensitivity of the sensors with 6.5 turns is approximately 2.29 times of that with 4.5 turns, and 4.83 times enhancement is achieved from change of 4.5 turns to 9.5 turns. The results illustrate the sensitivity of the sensor could be improved by increasing the turns of the coil.

For the line width of the sensor, three groups of sensors are fabricated with $n = 6.5$, and $DR = 1$. The sensitivity under these three conditions is calculated as shown in Fig. 5d. The sensitivity of the sensor with $w = 1, 1.5$, and 2 mm is in the ranges of 0.90–0.98%, 1.23–1.36%, and 1.49–1.65%, respectively. Since the DR of the sensor remains the same, the larger line width makes the sensor larger in size, which increases the change in mutual inductance between the straight wires. Therefore, the sensitivity could be improved by the increased line width.

The simulation calculation and experimental results show that the sensors in the folding deformation mode could achieve high sensitivity. Single-fold and three-fold sensors are fabricated to evaluate the effect of the number of folding on sensitivity. The 3D schematic is shown in Fig. 5e. The measurement results revealed that the average sensitivity of several three-fold sensors was 1.34 times that of single-fold sensors. The sensitivity of the sensor could be significantly improved by simply multiple folding.

Analysis of the effects of the above parameters on the sensitivity of the sensor and experimental verification demonstrate that the sensitivity could be improved by increasing n , increasing w , decreasing DR, adopting the regular quadrilateral shape, using the folding deformation mode, and increasing the number of folding units. Among them, changing the coil shape, adopting the folding deformation mode, and increasing the number of folding will not affect the size of the sensor. In terms of coil shape, the regular quadrilateral shape requires shorter coil length but with higher sensitivity. Therefore, the regular quadrilateral shape was selected as the optimal coil shape. The folding

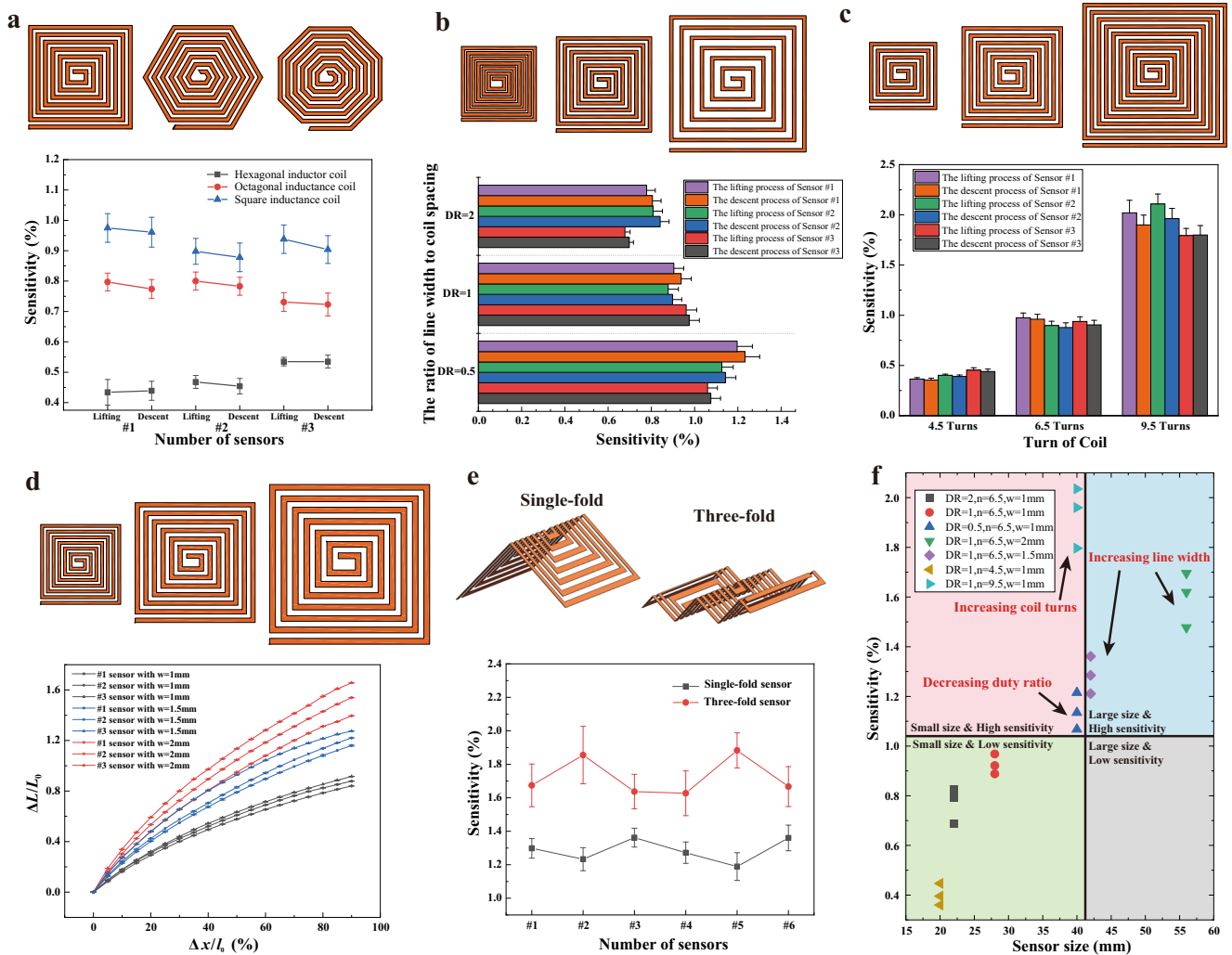


Fig. 5 Comparison and optimization of various parameters of PSIFS. a–e Schematic and sensitivity comparison of sensors with different coil shapes, duty ratio (DR), numbers of turns (n), line width (w), and numbers of folding units. **f** Comparison of the effect of different parameters on sensitivity-size two dimensions. The error bars in this figure are all defined as standard deviation.

deformation mode was determined similarly. In terms of increasing the number of folding units, introducing several folding units leads to multiple concave creases and convex creases. The inductance coil material located in the concave crease could be easily fractured due to compression strain, thus resulting in failure. Therefore, in comprehensive consideration of the practical application scenarios, the structural parameter $n = 1$ is adopted.

The method to improve sensitivity of the sensor by increasing the number of turns of coil, increasing the line width of coil, and decreasing DR, could lead to the enlargement of sensor size. Although the relative sensitivity was calculated for performance comparison, in which the size was considered to a certain extent, the absolute size of the sensor needs to be further considered because too large sensor size will restrict the portability and applicability of the sensor. Three methods for improving the performance are compared in the sensitivity and sensor size and results are shown in Fig. 5f. The abscissa represents the size of the sensor, and the ordinate represents the sensitivity of the sensor. These several methods are divided into four quadrants artificially. The comparison results showed that decreasing DR could control the sensor size to a certain extent, but the improvement of sensitivity is limited. The sensitivity could be improved by increasing the line width, but the sensor size is too large. Compared with the above two methods, increasing the number of

turns of coil controlled the sensor size well and achieved high sensitivity. The two-dimensional comparison shows that effect of increasing the number of turns is the optimal choice. Therefore, the design principle of PSIFS can be concluded through the above results. The use of regular quadrilateral shape and folding deformation can improve sensor sensitivity without increasing the sensor size. Increasing the number of turns of coil, increasing the line width of coil, and decreasing DR can also improve sensor sensitivity but increasing the sensor size meanwhile. Under sensitivity-size two dimensions, increasing the number of turns is a better choice than the other two.

Performances of PSIFS

In comprehensive consideration of the sensitivity and sensor size, the optimal configuration of structural parameters is obtained. A quadrilateral coil in 48 mm \times 48 mm was fabricated with parameters of $w = 1$ mm, DR = 1, and $n = 11.5$, and single folding operation. Given the particularity of the folding structure, it is difficult to be restored to the initial state by self-driven after fully unfolding. Therefore, the measurement range of PSIFS is set to 43.2 mm. First, displacement test was carried out in full range and the interval is 5% of the length of the sensor as 4.8 mm. The testing curve in different displacements is shown in Fig. 6a. Stable inductance value was maintained under different displacement

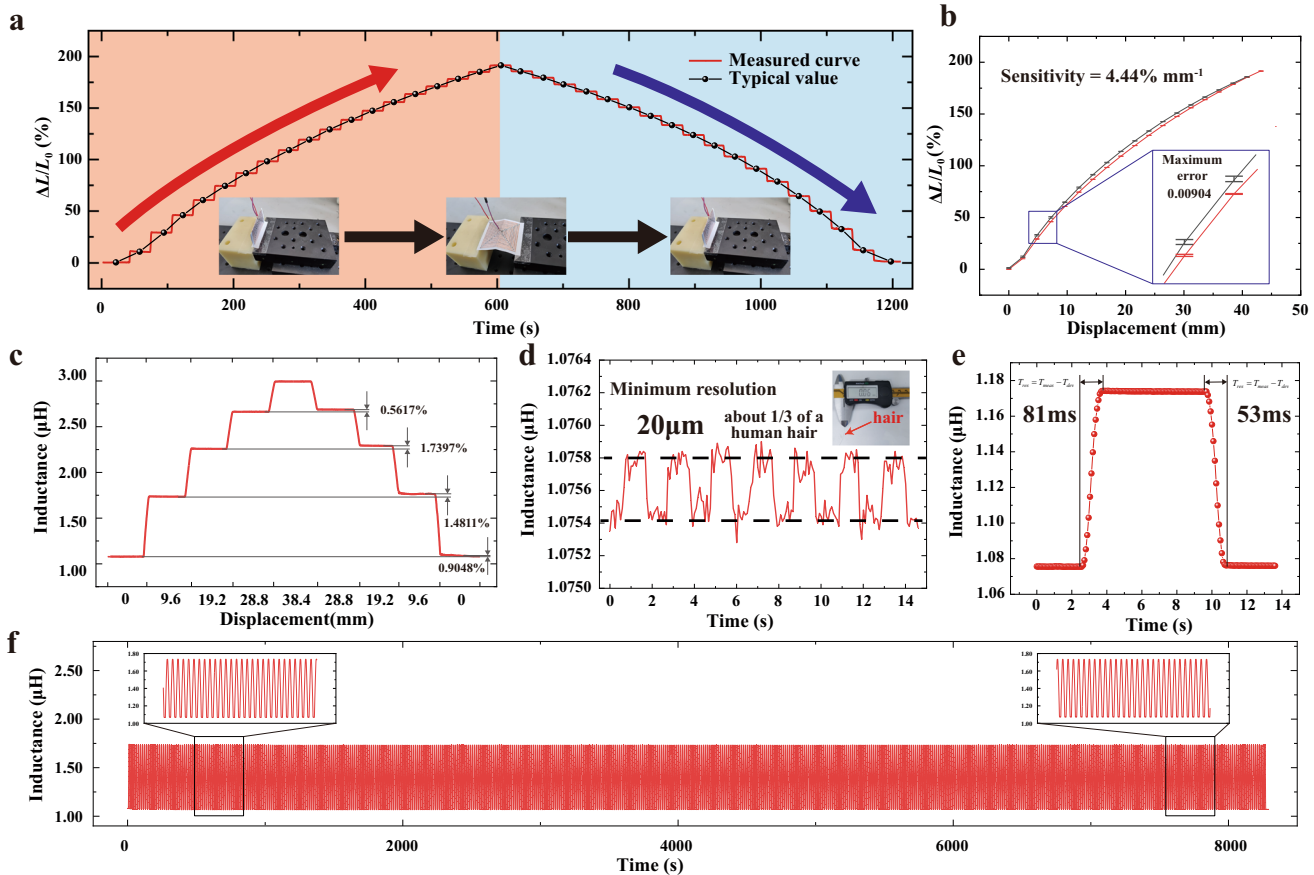


Fig. 6 Performance testing of PSIFS. **a** Measurement curve in full range. **b** Sensitivity curve and error PSIFS. The error bar shows the standard deviation. **c** Inductance variation curves of PSIFS at the same measurement position in lifting and returning. **d** Cycling test of PSIFS in minimum resolution displacement (20 μm). **e** Measurement curve of the response time of PSIFS. **f** Long-term stability test curve of PSIFS.

conditions and the numerical consistency also remained good in the process of lifting and returning.

The sensitivity curve is shown in Fig. 6b. The average sensitivity of PSIFS in full range is approximately $4.44\% \text{ mm}^{-1}$ at the full range of 0–43.2 mm. The measurement curve of the sensor basically shows a linear trend and the hysteresis is about 2.4%. Meanwhile, the sensitivity in small displacement measurement is slightly higher than that in large displacement measurement. The maximum error is only 0.00904 in the full range, which illustrates the precision of PSIFS. Moreover, with 0, 9.6, 19.2, and 28.8 mm as the marked displacement points, the maximum relative error in the same displacement is only 1.74%, as shown in Fig. 6c.

Due to the ultrasensitive characteristics of PSIFS, the minimum resolution of the sensor was evaluated as shown in Fig. 6d. In the testing process, PSIFS could reach a minimum resolution of 20 μm , which is approximately equal to 1/3 of human hair. In several cycle testing, a good consistency of inductance is also maintained in such small displacement variation. The wide measurement range and high resolution of the sensor proves that practical requirements could be both met in the small displacement and the large-range measurement. The response time of the sensor was also measured in 2.4 mm displacement. The precious displacement controller is used to determine the displacement to be measured, and time (T_{dev}) of 1.2 s is needed for the device to achieve 2.4 mm displacement. Thus, the response time of the sensor (T_{res}) should be $T_{\text{res}} = T_{\text{meas}} - T_{\text{dev}}$, where T_{meas} means the measured time. The measurement result shows that the response time of PSIFS in loading is about 81 ms, and the response time in relief is approximately 53 ms, as shown in Fig. 6e. In addition, we also test and calculate the response time of the sensor under 19.2 mm

displacement excitation, as shown in Supplementary Fig. 3. In this condition, the response time loading and unloading is 123 ms and 122 ms, respectively. Considering the errors of measuring the instrument and displacement controller, the response time of PSIFS is about 100 ms, which means good tracking could also be achieved for high-frequency motion signal measurement.

In addition, over 800 cycles were carried out in the displacement range of 0–9.6 mm, and long-term stability results can be seen in Fig. 6f. It can be found that the value of PSIFS only changed about -1.02% after over 800 cycle testing, which are calculated through difference between the cycled inductance and the initial inductance divided by the initial inductance. The results show that paper-based displacement sensor could maintain high stability in long-term applications. Besides, the influence of temperature and humidity disturbance on inductance of sensor. We put the temperature and humidity changing curve and the displacement (about 10 mm) changing curve in same figures, as Supplementary Fig. 4. It can be seen that the inductance value of PSIFS drifts about 0.2% when the temperature changes of 10°C , which means measured displacement error of only 0.045 mm. The inductance value of the sensor drifts about 2.5% when the humidity changes of 40%, which means measured displacement error of 0.568 mm. It can be seen from the results that although disturbance has an impact on the inductance value of PSIFS, the temperature and humidity drift can be almost ignored compared with displacement signals. Some additional experiments are also operated to verify the robustness of PSIFS itself. After 1000 cycles of full range, there is nearly no plastic deformation in the folding crease. For the adhesion between the copper coil and the paper

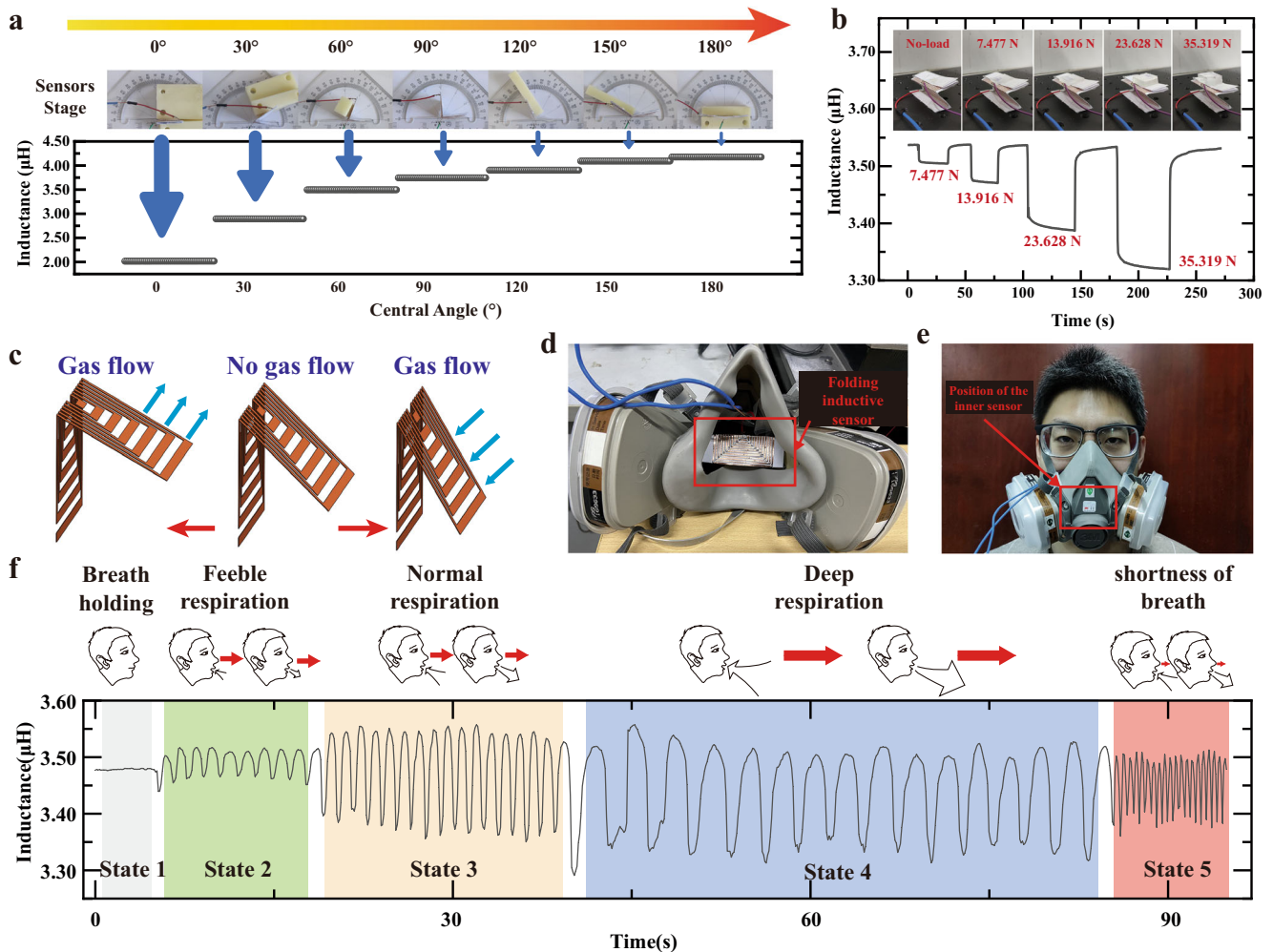


Fig. 7 Various applications of PSIFS. **a** Measurement results of different angles. **b** Measurement results of different pressure. **c** Schematic of the principle of respiratory monitoring. **d** Position of the sensor in breathing mask. **e** Pictures of breathing mask and sensor in the practice. **f** Monitoring results of PSIFS in different breathing modes.

substrate, there is no unsticking phenomenon after fabricating five convex creases and four concave creases.

Practical applications of PSIFS

Due to the crease hinge function in folding structure, the rotation of angle could be presented as the displacement change between two ends of the sensor. PSIFS could produce a distinguishable response when placed at different angles as shown in Fig. 7a. In the process of completely bending to fully unfolding, the angle changed from 0° to 180° , and the inductance value of the sensor increased gradually. PSIFS is more sensitive in small-angle state and this changing trend is consistent with simulation result in Fig. 3b. PSIFA with the same size of the simulation structure is also fabricated and the inductance values of the two at different angles are shown in Supplementary Fig. 5. Both the variation trend and numerical values are consistent.

Moreover, the pressure could also be measured using force-displacement transformation of the folding structure. Based on the law of elasticity, the folding structure deforms under the action of force, resulting in the displacement change between two ends of PSIFS. According to this principle, one end of PSIFS was fixed, while the other end was suspended as a mover to measure the pressure input. The sensor could achieve a good resolution of different pressure as shown in Fig. 7b. PSIFS also could be restored to the no-load state after the pressure was removed. The above

results show that PSIFS has the potential for pressure measurement.

PSIFS has short response time, high sensitivity and capacity of angle degree and pressure measurement, which shows the potential to monitor human respiration. As shown in Fig. 7c, one end of the sensor was fixed, while the other end suspended. When a person breathes in, the movable end of PSIFS is driven to move outward. Accordingly, both the angle of the folding structure and the sensor inductance increase. When breathing out, the movable end of the sensor is driven to squeeze inward. Accordingly, the inductance of PSIFS decreases with the angle decreasing. Therefore, PSIFS could be used to monitor respiration states. The installation position of PSIFS in the mask is shown in Fig. 7d and wearing scenario is shown in Fig. 7e. Due to that the paper substrate and copper coil are both harmless to humans and the environment, PSIFS allows for the harmless and long-term wearing and measurement.

Many diseases are often accompanied by ragged breathing, weak breathing, and other characteristics of the human respiration. Therefore, PSIFS was tested for monitoring various respiration states, as shown in Fig. 7f. The actual monitoring process can be seen in Supplementary Video 1. First, when breath was held and the sensor was left in natural state, the inductance value of the sensor is represented as a section of approximately horizontal straight line on the curve, as shown in State 1. In weak breathing,

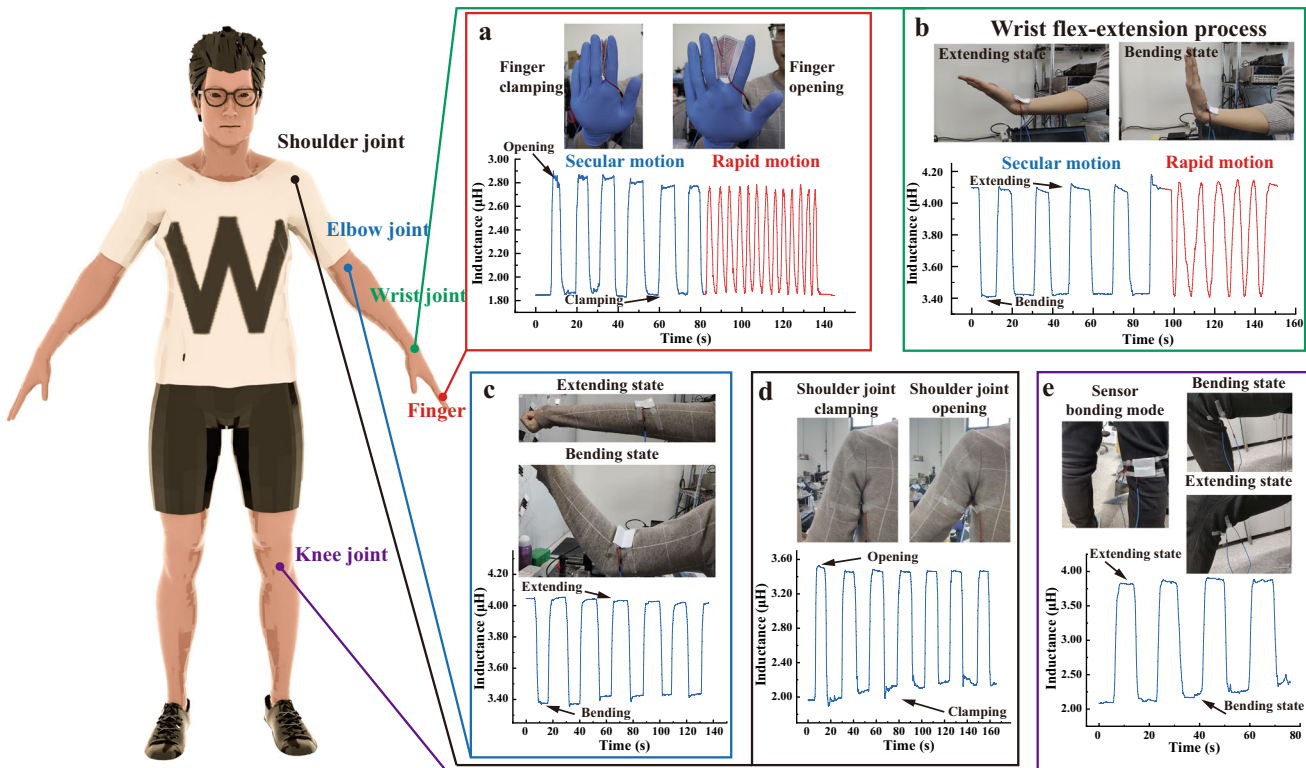


Fig. 8 Application of PSIFS in human motion monitoring. a–e Measurement results of finger opening and closing, wrist flex-extension, elbow joint rotation, shoulder joint rotation, and knee joint rotation.

the inductance value of PSIFS changed slightly and regularly with the breathing, as shown in State 2. In normal breathing as State 3, the intensity of breath-in and breath-out was higher than that in the weak breathing state, which was consistent with the change of respiration states. In the measurement curve of the sensor as State 4, the intensity and cycling time of deep breathing were both higher than that of normal breathing, which corresponds to actual breathing characteristics. Finally, rapidly breathing was tested and the curve demonstrated that the inductance variation range of PSIFS was slightly smaller than that in normal breathing and deep breathing. In addition, the frequency of periodic change in inductance value was the highest in these cases, which was consistent with the subjects' breathing. Therefore, PSIFS could achieve monitoring of multiple respiration state and had the potential for respiratory measurement during illness or exercise.

To verify the robustness of PSIFS, the disturbance of head movement during the breath monitoring was tested. The interference activities included head moving up, down, left and right respectively. When the head moving, the subject held his breathing. The results are shown in Supplementary Fig. 6. Although the inductance of PSIFS changed a little when introducing disturbance, it is much smaller than the breathing caused and the breathing signal can still be distinguished easily.

In addition to the monitoring of human respiration, PSIFS could also be used in monitoring human motion. The parts of the human body commonly used during exercise, including fingers, wrists, elbows, shoulders, and legs, are selected for experiments. First, PSIFS was stuck in the middle of fingers. When fingers opened and closed, they could drive the displacement change at both ends of PSIFS, which was represented as the change of inductance value, as shown in Fig. 8a. For the flex-extension of the wrist, PSIFS was fixed on the wrist joint of the human body, with one end fixed on the palm and the other end fixed on the upper of the forearm. When the wrist was overturned, the distance between two ends of the sensor changed regularly, as shown in

Fig. 8b. Because the situations of fast motion could usually occur in these two kinds of motion modes, the changes in fast motion were tested. Results show that PSIFS could reach a good resolution in normal motion and fast motion.

In addition, two ends of PSIFS were fixed on both arms to measure the movement of elbow joint. PSIFS could recognize the overturning of wrist well, as shown in Fig. 8c. For measurement of the shoulder joint, two ends of PSIFS are fixed on the upper arm and the inside of the trunk, with the crease part of PSIFS placed under the armpit. When the movement of the shoulder joint drove the arm to rotate, the distance between two ends of PSIFS also changes, so the monitoring could be realized as shown in Fig. 8d. Leg is also one of the important motion organs depending on knee joint bending". PSIFS was fixed between the thigh and lower leg to test the bending motion of knee joint and the test results reveal that the sensor could monitor leg flexion well, as shown in Fig. 8e.

The above test results show that PSIFS could monitor the respiration as well as the movement of fingers, wrist joints, elbow joints, shoulder joints, and knee joints. The actual monitoring process can be seen in Supplementary Video 2–6. It could be used for signal monitoring whether directly fixed on the surface of human skin or combined with clothing, gloves, masks, and other wearable garments. Therefore, PSIFS shows the high practical value for electronic skin and wearable devices.

The comparison between PSIFS and other sensors is shown in Table 1. The measurement principle of PSIFS is based on the change in the inductance value of the coil. Therefore, wireless measurement is expected to be realized through reasonable circuit design in the future to further demonstrate the advantages. Due to simple processing of paper materials, the leading wire position could be changed to meet different application requirements, so as to better suit for the wearable motion monitoring. For example, the electrode material could be introduced to the reverse side of the sensor to avoid the inconvenience caused by the leading wire in the center of the sensor, as shown in

Table 1. The comparison of this work with other work.

Research	Sensor type	Substrate materials	Sensor size & Shape	Max range	Displacement sensitivity	Angle sensitivity
Ref. ²⁴	Self-inductive sensor	Polyester	7.5 mm*50 mm (Plat)	15 mm	1.14% mm ⁻¹	0.17% ° ⁻¹
Ref. ⁴⁷	Self-inductive sensor	Polyimide	50 mm*50 mm (Plat)	25 mm	0.43% mm ⁻¹	Unknown
Ref. ⁴⁸	Resistive sensor	Rubber	Φ3mm*52 mm (Tube)	50 mm	~2% mm ⁻¹	~0.21% ° ⁻¹
Ref. ⁴⁹	Electromagnetic sensor	Polyimide	Φ25mm (Plat)	Unknown	0.00059 mV mm ⁻¹	Unknown
Ref. ⁵⁰	TENG sensor	Kapton	10 mm*120 mm (Plat)	Unknown	~4% mm ⁻¹	Unknown
This work	Self-inductive sensor	Paper	48 mm*48 mm (Plat)	43.2 mm	4.44% mm ⁻¹	0.60% ° ⁻¹

Supplementary Fig. 7. The experimental results have proved the robustness of PSIFS in applications. For the more extreme scenarios, the additional coating (Parylene C etc.) could be used to increase the sensor lifetime further.

DISCUSSION

An environment-friendly, economic, and high-performance PSIFS was proposed in this paper. Paper material and copper tape were used as the substrate and the coil layer and the manufacturing process can be achieved without complex fabrication process. Calculation and simulation analysis were carried out to explain the sensing mechanism of PSIFS. Using the proposed folding method to enhance sensitivity, it is proved by experiment that the sensitivity could be increased to 3 times by once folding. The design principle of multiple structure parameters of planar inductor coil on the sensitivity-size two dimensions was proposed, including coil shape, duty ratio (DR), coil turns (n) and line width (w). After the optimal parameter setting, the average sensitivity of PSIFS could reach 4.44% mm⁻¹ under the full range of 0–43.2 mm. The minimum displacement resolution could reach 20 μm and PSIFS also maintained small hysteresis (2.4%) and short response time (<100 ms). In addition, the maximum relative error in full range is only 0.00904. PSIFS also showed excellent stability in the long-term fatigue test, with only 2.5% deviation after over 800 cycling tests. PSIFS could also be used to measure the angle degree and pressure due to its folding structure, and the sensitivity of angle degree could reach 0.60% per degree. PSIFS could also monitor the respiratory rate and amplitude. Different respiration modes, including breath holding, feeble, normal respiration deep respiration and shortness of breath, could be recognized clearly. As a wearable sensor, PSIFS could be used to measure fingers, wrist joints, elbow joints, shoulder joints, and knee joints motion signals. Overall, by using the folding structure of paper material, PSIFS shows high sensitivity and also has a very simple and economic fabrication process. The proposed simple paper-based sensor, folding method to increase sensitivity, and design model are expected to provide possible ways for the research of flexible sensors.

METHODS

Manufacturing process of PSIFS

A4 paper (No. 7362, Deli) was selected as the flexible substrate, thickness of which was approximately 80 μm. Paper was modified to the required size and shape by using a cutting tool (No. 8016, Deli). PSIFS was in a regular quadrilateral shape, with a size of 48 mm × 48 mm. Copper, with strong conductivity and high economy, was selected as the material of the coil. The copper foil tape (thickness of 65 μm) was used and cut into the corresponding size with scissors in accordance with the length of each side and the line width of the coil. Then, it was stuck on the flexible substrate to form the coil shape. Solder (Sn60Pb40, SANKI) was introduced to connect the units and achieve good conductivity between copper foil units. The leading wires (30AWG) connected to the inductance coil with solder were used for the measurement of electrical signal.

The performance measurement and human physiological signal monitoring

Precise electric displacement controller (Model Z825B, Thorlabs) was used to control the displacement of the sensor. Precision impedance analyzer (Model WK6500B, Wayne Kerr) was used to measure the inductance of the sensor. Temperature and humidity chamber (Model HT-S-50L, Changxu) was used to control the condition of temperature and humidity. During the pressure testing, neither conductive nor magnetic PDMS blocks with different mass were used as pressure input. For human respiratory monitoring, the sensor was fixed in the mask (Model 6001CN, 3M). The breathing state of the subject could be monitored by observing the real-time inductance value of the sensor. For monitoring the human motion signal, the sensors were pasted on the skin or clothes by the medical PE tape (LEAGUE). The experiment in this paper only involves the collection of common human motion signals without the ethical part, and informed written consent from all participants was obtained prior to the research.

DATA AVAILABILITY

The data that support the finding of this study are available from the corresponding author upon reasonable request.

CODE AVAILABILITY

The codes that support the finding of this study are available from the corresponding author upon reasonable request.

Received: 15 December 2021; Accepted: 10 July 2022;

Published online: 02 August 2022

REFERENCES

- Ma, J. H. et al. Highly sensitive and large-range strain sensor with a self-compensated two-order structure for human motion detection. *ACS Appl. Mater. Interfaces* **11**, 8527–8536 (2019).
- Yan, Z. C. et al. Stretchable micromotion sensor with enhanced sensitivity using serpentine layout. *ACS Appl. Mater. Interfaces* **11**, 12261–12271 (2019).
- Ramirez, J., Rodriguez, D., Urbina, A. D., Cardenas, A. M. & Lipomi, D. J. Combining high sensitivity and dynamic range: Wearable thin-film composite strain sensors of Graphene, Ultrathin Palladium, and PEDOT:PSS. *ACS Appl. Nano Mater.* **2**, 2222–2229 (2019).
- Thuruthel, T. G., Shih, B., Laschi, C. & Tolley, M. T. Soft robot perception using embedded soft sensors and recurrent neural networks. *Sci. Robot.* **4**, 1488 (2019).
- Bauer, S. et al. 25th Anniversary Article: A Soft Future: From Robots and Sensor Skin to Energy Harvesters. *Adv. Mater.* **26**, 149–162 (2014).
- Zhao, H. C., O'Brien, K., Li, S. & Shepherd, R. F. Optoelectronically innervated soft prosthetic hand via stretchable optical waveguides. *Sci. Robot.* **1**, 7529 (2016).
- Wang, S. H. et al. Skin electronics from scalable fabrication of an intrinsically stretchable transistor array. *Nature* **555**, 83 (2018).
- Duan, Z. H. et al. Facile, Flexible, Cost-Saving, and Environment-Friendly Paper-Based Humidity Sensor for Multifunctional Applications. *ACS Appl. Mater. Interfaces* **11**, 21840–21849 (2019).
- Ho, D. H. et al. Crack-Enhanced Microfluidic Stretchable E-Skin Sensor. *ACS Appl. Mater. Interfaces* **9**, 44678–44686 (2017).
- Jeong, H., Noh, Y., Ko, S. H. & Lee, D. Flexible resistive pressure sensor with silver nanowire networks embedded in polymer using natural formation of air gap. *Compos. Sci. Technol.* **174**, 50–57 (2019).

11. Chang, H. et al. Ultrasensitive and Highly Stable Resistive Pressure Sensors with Biomaterial-Incorporated Interfacial Layers for Wearable Health-Monitoring and Human-Machine Interfaces. *ACS Appl. Mater. Interfaces* **10**, 1067–1076 (2018).
12. Huang, Y., Fan, X. Y., Chen, S. C. & Zhao, N. Emerging Technologies of Flexible Pressure Sensors: Materials, Modeling, Devices, and Manufacturing. *Adv. Funct. Mater.* **29**, 1808509 (2019).
13. Xu, H. H. et al. An ultra-stretchable, highly sensitive and biocompatible capacitive strain sensor from an ionic nanocomposite for on-skin monitoring. *Nanoscale* **11**, 1570–1578 (2019).
14. Kim, H. et al. Transparent, Flexible, Conformal Capacitive Pressure Sensors with Nanoparticles. *Small* **14**, 1703402 (2018).
15. Sriphan, S. et al. Flexible capacitive sensor based on 2D-titanium dioxide nanosheets/bacterial cellulose composite film. *Nanotechnology* **32**, 155502 (2021).
16. Wang, Y. et al. Three-dimensional stretchable microelectronics by Projection Microstereolithography (PmuSL). *ACS Appl. Mater. Interfaces* **13**, 8901–8908 (2021).
17. Biswas, D. K. et al. Modeling and characterization of scaling factor of flexible spiral coils for wirelessly powered wearable. *Sens. Sens.* **20**, 2282 (2020).
18. Nie, B. et al. Textile-Based Wireless Pressure Sensor Array for Human-Interactive Sensing. *Adv. Funct. Mater.* **29**, 1808706 (2019).
19. Jang, C.-I. et al. Effects of inner materials on the sensitivity and phase depth of wireless inductive pressure sensors for monitoring intraocular pressure. *Appl. Phys. Lett.* **108**, 103701 (2016).
20. Tang, X., Miao, Y., Chen, X. & Nie, B. A Flexible and Highly Sensitive Inductive Pressure Sensor Array Based on Ferrite Films. *Sensors* **19**, 2406 (2019).
21. He, X. et al. An ultrathin paper-based self-powered system for portable electronics and wireless human-machine interaction. *Nano Energy* **39**, 328–336 (2017).
22. Kawasetsu, T., Niyama, R., Kuniyoshi, Y. & Ieee. Flexible and Soft Inductive Tri-axis Tactile Sensor Using Liquid Metal as Sensing Target. *2019 IEEE Sens.* 5834–5841 (2019).
23. Jerance, N., Vasiljevic, D., Samardzic, N. & Stojanovic, G. A Compact Inductive Position Sensor Made by Inkjet Printing Technology on a Flexible Substrate. *Sensors* **12**, 1288–1298 (2012).
24. Moreton, G., Meydan, T., Williams, P. Investigation and characterization of a planar figure-of-eight coil as a curvature sensor. *2019 IEEE Sens.* 786–788 (2017).
25. Prituja, A. V., Banerjee, H. & Ren, H. Electromagnetically Enhanced Soft and Flexible Bend Sensor: A Quantitative Analysis With Different Cores. *IEEE Sens. J.* **18**, 3580–3589 (2018).
26. Zhang, F., Wu, S. Y., Peng, S. H., Sha, Z. & Wang, C. H. Synergism of binary carbon nanofibres and graphene nanoplates in improving sensitivity and stability of stretchable strain sensors. *Compos. Sci. Technol.* **172**, 7–16 (2019).
27. Kumaresan, Y., Ma, S., Ozioko, O. & Dahiya, R. Soft Capacitive Pressure Sensor With Enhanced Sensitivity Assisted by ZnO NW Interlayers and Airgap. *IEEE Sens. J.* **22**, 3974–3982 (2022).
28. Ye, Z., Li, Q., Zhang, R., Zhang, P. & Gui, L. Fabrication of a thin PDMS film with complex liquid metal electrodes embedded and its application as skin sensors. *RSC Adv.* **12**, 8290–8299 (2022).
29. Jia, M. et al. Hierarchical Network Enabled Flexible Textile Pressure Sensor with Ultrabroad Response Range and High-Temperature Resistance. *Adv. Sci.* (2022).
30. Zeng, Z.-H. et al. Porous and Ultra-Flexible Crosslinked MXene/Polyimide Composites for Multifunctional Electromagnetic Interference Shielding. *Nano-Micro Lett.* **14**, 1–16 (2022).
31. Li, R. Z., Hu, A., Zhang, T. & Oakes, K. D. Direct writing on paper of foldable capacitive touch pads with silver nanowire inks. *ACS Appl. Mater. Interfaces* **6**, 21721–21729 (2014).
32. Santhiago, M. et al. Flexible and Foldable Fully-Printed Carbon Black Conductive Nanostructures on Paper for High-Performance Electronic, Electrochemical, and Wearable Devices. *ACS Appl. Mater. Interfaces* **9**, 24365–24372 (2017).
33. Najafabadi, A. H. et al. Biodegradable nanofibrous polymeric substrates for generating elastic and flexible electronics. *Adv. Mater.* **26**, 5823–5830 (2014).
34. Emamian, S., Narakathu, B. B., Chlaihawi, A. A., Bazuin, B. J. & Atashbar, M. Z. Screen printing of flexible piezoelectric based device on polyethylene terephthalate (PET) and paper for touch and force sensing applications. *Sens. Actuators A-Phys.* **263**, 639–647 (2017).
35. Iglío, R., Mariani, S., Robbiano, V., Strambini, L. & Barillaro, G. Flexible Polydimethylsiloxane Foams Decorated with Multiwalled Carbon Nanotubes Enable Unprecedented Detection of Ultralow Strain and Pressure Coupled with a Large Working Range. *ACS Appl. Mater. Interfaces* **10**, 13877–13885 (2018).
36. Chen, W., Feng, F., Chen, D., Lin, W. & Chen, S.-C. Precision non-contact displacement sensor based on the near-field characteristics of fiber specklegrams. *Sens. Actuator A-Phys.* **296**, 1–6 (2019).
37. Chen, Z. et al. Enhancing the sensitivity of percolative graphene films for flexible and transparent pressure sensor arrays. *Adv. Funct. Mater.* **26**, 5061–5067 (2016).
38. Adepu, V., Kamath, K., Mattela, V. & Sahatiya, P. Laser-Assisted Gaussian Microstructure Patterned PDMS Encapsulated Ti-3 C-2 T-x (MXene)-Based Pressure Sensor for Object and Touch Detection. *IEEE Sens. J.* **21**, 16547–16553 (2021).
39. Huang, Q. et al. Protrusion microstructure-induced sensitivity enhancement for zinc oxide-carbon nanotube flexible pressure sensors. *ACS Appl. Electron. Mater.* **3**, 5506–5513 (2021).
40. Liu, Z. Y. et al. Surface strain redistribution on structured microfibers to enhance sensitivity of fiber-shaped stretchable strain sensors. *Adv. Mater.* **30**, 1704229 (2018).
41. Kumar, S., Ropmay, G. D., Rathore, P. K., Rangababu, P. & Akhtar, J. Sensitivity enhancement of P- and N-MOS based current mirror pressure sensor using differential amplifier. *A two-day conference flexible electronics electric Vehicles.* **2294**, 020002 (2020).
42. Chen, S. et al. Flexible and transparent sensors with hierarchically micro-nano texture for touchless sensing and controlling. *Nano Energy* **82**, 105719 (2021).
43. Greenhouse, H. M. Design of planar rectangular microelectronic inductors. *IEEE Trans. Parts, Hybrids, Packag.* **PH10**, 101–109 (1974).
44. Aebischer, H. A. Inductance formula for square planar spiral inductors with rectangular conductor cross section. *Adv. Electromagnetics* **8**, 80–88 (2019).
45. Luo, Z. & Wei, X. Analysis of square and circular planar spiral coils in wireless power transfer system for electric vehicles. *IEEE Trans. Ind. Electron.* **65**, 331–341 (2018).
46. Tavakkoli, H., Abbaspour-Sani, E., Khalilzadegan, A., Abazari, A.-M. & Rezaezadeh, G. Mutual inductance calculation between two coaxial planar spiral coils with an arbitrary number of sides. *Microelectron. J.* **85**, 98–108 (2019).
47. Babkovic, K., Damnjanovic, M., Nagy, L., Kisic, M. & Stojanovic, G. Inductive Displacement Sensor of Novel Design Printed on Polyimide Foil. *IEEE Trans. Magn.* **53**, 4001505 (2017).
48. Dohta, S., Akagi, T., Kuno, H. & Hamamoto, I. Development of string-type flexible displacement sensor to measure the movement of robot and human body. *Int. J. Intell. Syst.* **8**, 86–99 (2010).
49. Zhao, Y. et al. Fully Flexible Electromagnetic Vibration Sensors with Annular Field Confinement Origami Magnetic Membranes. *Adv. Funct. Mater.* **30**, 2001553 (2020).
50. Yuan, Z., Shen, G., Pan, C. & Wang, Z. L. Flexible sliding sensor for simultaneous monitoring deformation and displacement on a robotic hand/arm. *Nano Energy* **73**, 104764 (2020).

ACKNOWLEDGEMENTS

This work was financially supported by National Natural Science Foundation of China Project (No. 52075291, 61671271 and 51735007).

AUTHOR CONTRIBUTIONS

X.Y. and J.Z. conceived the idea and designed the project scheme. J.Z. designed experiments and wrote the manuscript. Y.J., Y.L., Z.Z., and Y.C. helped in some parts of experiments. X.Y. and Q.L. polished and revised the manuscript. All authors reviewed the manuscript.

COMPETING INTERESTS

The authors declare no competing interests.

ADDITIONAL INFORMATION

Supplementary information The online version contains supplementary material available at <https://doi.org/10.1038/s41528-022-00198-0>.

Correspondence and requests for materials should be addressed to Xing Yang.

Reprints and permission information is available at <http://www.nature.com/reprints>

Publisher's note Springer Nature remains neutral with regard to jurisdictional claims in published maps and institutional affiliations.



Open Access This article is licensed under a Creative Commons Attribution 4.0 International License, which permits use, sharing, adaptation, distribution and reproduction in any medium or format, as long as you give appropriate credit to the original author(s) and the source, provide a link to the Creative Commons license, and indicate if changes were made. The images or other third party material in this article are included in the article's Creative Commons license, unless indicated otherwise in a credit line to the material. If material is not included in the article's Creative Commons license and your intended use is not permitted by statutory regulation or exceeds the permitted use, you will need to obtain permission directly from the copyright holder. To view a copy of this license, visit <http://creativecommons.org/licenses/by/4.0/>.